International Journal of Thermophysics (2025) 46:95
https://doi.org/10.1007/s10765-025-03565-x

An Accurate Thermodynamic Model to Characterise Dissociating N_2O_4 at Vapour–Liquid Equilibrium States

Konstantin Samukov[1] · David Vega-Maza[2] · Eric W. Lemmon[3] · Vladimir Diky[3] · Silvia Lasala[1]

Received: 26 March 2025 / Accepted: 19 April 2025 / Published online: 10 May 2025

Abstract

A new thermodynamic model is presented, capable of accurately representing the vapour–liquid equilibrium pressures and densities, and liquid phase densities and enthalpies of dissociating dinitrogen tetroxide ($N_2O_4 \rightleftarrows 2NO_2$). The model is based on the Peng-Robinson equation of state coupled with advanced mixing rules. The -required but non-measurable- critical coordinates of the pure components forming the reactive mixtures are optimized, within a variability range defined in a previous study, to fit experimental vapour–liquid equilibrium data. The optimized parameters are then validated by comparing calculated thermodynamic properties with available experimental data in the subcritical region. The negligible impact of the higher temperature reaction $2NO_2 \rightleftarrows 2NO + O_2$, within the vapour–liquid equilibrium region where the optimisation is performed, is also proven. The resulting model is finally compared with the currently most accurate available equation of state, showing comparable results when considered both the scatter in available experimental data and the relative simplicity of the proposed equation of state. In particular, the proposed model demonstrates the satisfactory capability of a cubic equation of state to accurately reproduce both saturation pressures and saturation densities without requiring volume translation.

Keywords Chemical equilibrium · Dinitrogen tetroxide · Equation of state · Reactive mixtures · Vapour–liquid equilibrium

(Eric W. Lemmon and Vladimir Diky) Any mention of commercial products within this article is for information only; it does not imply recommendation or endorsement by NIST. These opinions, recommendations, findings, and conclusions do not necessarily reflect the views or policies of NIST or the United States Government.

Extended author information available on the last page of the article

1 Introduction

When in 1957 Lighthill [1] proposed to convert the energy of dissociating gases into work, the use of N_2O_4 as a working fluid for power plants became a curiosity that researchers started to explore [2–7]. The N_2O_4 strong oxidizing capacity was also known, enabling its combination with the hydrazine family of fuels for rocket propulsion [8–10]. The benefits associated with the utilization of N_2O_4 in nuclear power plants were mainly investigated through research conducted at the Nuclear Power Institute of the Academy of Sciences of the Byelorussian SSR from 1960 to 1985. This Institute performed thorough studies on the reactive system $N_2O_4 \rightleftarrows 2NO_2 \rightleftarrows 2NO + O_2$, measuring its thermodynamic and transport properties in a wide range of temperature and pressure [11–13], assessing thermodynamic cycles performance theoretically and experimentally [3, 14], and investigating heat exchange processes [15, 16].

From this time to 1990, other researchers have analysed the effect of using N_2O_4 as a working fluid in thermodynamic cycles; a review of existing studies was conducted in Lasala et al. [17, 18]. Calculations have shown that thermodynamic cycles operating with reactive working fluids are more efficient than traditional ones based on inert fluids (H_2O, He, and CO_2). Furthermore, the reactive system $N_2O_4 \rightleftarrows 2NO_2$ has advantages in terms of heat exchange properties: comparing it with hypothetical mixtures of non-reacting N_2O_4 and NO_2, it has been shown that the presence of the chemical reaction increases the heat capacity of a gas-phase mixture of N_2O_4 and NO_2 up to 1000 % [19–24], the thermal conductivity up to 800 % [24–27], and the heat transfer coefficient up to 900 % [28, 29]. However, this research area died away until some researchers started revising it, proposing a multipronged approach based on fundamental thermodynamics [30], chemical reaction and plant design engineering [31], and computational fluid dynamic investigations [29]. Interest in the system $N_2O_4 \rightleftarrows 2NO_2$ resurfaced; however, a practical and accurate thermodynamic model of the system was still lacking.

Dinitrogen tetroxide (N_2O_4) rapidly dissociates into two molecules of NO_2, or associates back to N_2O_4, as temperature increases or decreases, respectively, within the temperature range of approximately 260–415 K [32, 33]. The evolution of the reaction $N_2O_4 \rightleftarrows 2NO_2$ is dictated by the fast chemical equilibrium kinetics after a change of temperature and pressure. The dissociation of the dimer N_2O_4 and the association of two NO_2 monomers are considered fast reactions: the relaxation time in a gas phase at pressures above 1 bar does not exceed 10^{-4} s [34–39]. Experimental measurements and molecular dynamics simulations conducted in the liquid phase have revealed that the reaction is likewise rapid: half-life times calculated from experimentally determined rate constants by Bauer et al. [40] fall within the range of 10^{-6} to 10^{-4} s, while molecular dynamics simulations by Katō [41] yielded a lifetime of approximately 10^{-7} s. Moreover, above about 420 K and at very low pressures for all temperatures in the vapour phase, the second reaction $2NO_2 \rightleftarrows 2NO + O_2$ takes place and NO_2 is totally dissociated at about 875 K [32, 33].

In the previous paper by Lasala et al. [30], we addressed the challenges of modeling fluid phase equilibrium properties of dimerization reactions of type $A_n \rightleftarrows (n/m)A_m$ by proposing a multi-scale methodology that was specifically applied to the binary reactive system $N_2O_4 \rightleftarrows 2NO_2$. This previous paper shows a characteristic feature of binary reactive mixtures: similar to pure substances, the system has a unique triple point, a unique critical point and a phase envelope where bubble and dew loci overlap to form a single "saturation" pressure–temperature curve, even though the composition changes at each point and in each phase, according to chemical equilibrium. This fact is explained by the monovariance of the binary reactive fluid at vapour–liquid equilibrium (VLE), coincident with that of a pure fluid at saturation. In order to model the thermodynamic properties of the system with a cubic equation of state, the knowledge of critical coordinates, acentric factors and ideal gas properties of the molecules forming the mixture are required. The experimental determination of critical properties of pure N_2O_4 and NO_2 is not possible because of the occurrence of the chemical reaction $N_2O_4 \rightleftarrows 2NO_2$ over all VLE states. To overcome this problem, we performed Monte Carlo simulations to determine the critical properties and acentric factors of the pure NO_2 and N_2O_4. The ideal-gas properties of the two molecules were calculated by Quantum Mechanics simulations. Such a methodology is predictive in the sense that each input property is not optimized on experimental data but calculated by quantum and molecular approaches.

In order to increase the accuracy of the model, this paper aims, firstly, to investigate the influence of the critical properties of pure N_2O_4 and NO_2, previously estimated by Lasala et al. [30], on the results of calculations of the thermodynamic properties of the reactive system. Secondly, the optimal values of these critical properties, i.e., the values that maximize the accuracy of the thermodynamic model with respect to available data, are obtained and provided. Available chemical equilibrium experimental data demonstrate that NO_2 decomposition ($2NO_2 \rightleftarrows 2NO + O_2$) is negligible in the subcritical domain [42–49]. That has been validated in this study, where the optimization of the model is performed within the subcritical domain, considering only the presence of the reaction $N_2O_4 \rightleftarrows 2NO_2$; the impact of considering the occurrence of $2NO_2 \rightleftarrows 2NO + O_2$ is then assessed over the subcritical and supercritical domains. After introducing in Sect. 2 the methodology that has been followed, this paper presents the results in Sect. 3.

2 Methodology

The thermodynamic model and algorithms used to represent the system at chemical equilibrium are presented in Sects. 2.1 and 2.2, respectively. Section 2.3 reviews the available experimental data from the literature used in this methodology. Section 2.4 introduces the methodology for optimizing the critical coordinates of pure components to be used as an input to the thermodynamic model.

2.1 Modelling Chemical Equilibrium for the Systems $N_2O_4 \rightleftarrows 2NO_2$ and $N_2O_4 \rightleftarrows 2NO_2 \rightleftarrows 2NO + O_2$

A single-reaction reactive system at chemical equilibrium is characterized by a zero-Gibbs energy of reaction, $\Delta_R G$, that corresponds to the minimum of the Gibbs energy of the system, G, with the extent of reaction variable, ξ, for a specific temperature, T, and pressure, P [50, 51]:

$$\Delta_R G = \left(\frac{\partial G}{\partial \xi}\right)_{T,P} \overset{Chem.\ equil.}{=} 0 \tag{1}$$

In the case where the standard state chosen for each species is the pure ideal gas at temperature T and standard pressure P°, which is the standard state that must be chosen when calculations are carried out with an equation of state, this condition translates in the following expression,

$$K(T)_R = \prod_{i=N_{comp}} \left(\frac{\hat{f}_i}{P^\circ}\right)^{\nu_i} \tag{2}$$

where $\hat{f}_i$ is the fugacity of component i, ν_i is the stoichiometric number of component i, and the equilibrium constant of the reaction R, $K(T)_R$, is related by its definition to the standard Gibbs energy of the considered reaction, $\Delta_R G^\circ(T)$:

$$\ln K(T)_R = -\frac{\Delta_R G^\circ(T)}{RT} \tag{3}$$

The condition of chemical equilibrium, Eq. 2, of the reaction $N_2O_4 \rightleftarrows 2NO_2$ may be rewritten as:

$$K(T)_{N_2O_4 \rightleftarrows 2NO_2} = \frac{1}{P^\circ} \prod_{i=N_2O_4,NO_2} \hat{f}_i^{\nu_i} = \frac{1}{P^\circ} \cdot \frac{\hat{f}_{NO_2}^2}{\hat{f}_{N_2O_4}} \tag{4}$$

The condition for chemical equilibrium of the reaction $2NO_2 \rightleftarrows 2NO + O_2$ may be rewritten as:

$$K(T)_{2NO_2 \rightleftarrows 2NO + O_2} = \frac{1}{P^\circ} \prod_{i=NO_2,NO,O_2} \hat{f}_i^{\nu_i} = \frac{1}{P^\circ} \cdot \frac{\hat{f}_{NO}^2 \cdot \hat{f}_{O_2}}{\hat{f}_{NO_2}^2} \tag{5}$$

If both reactions occur simultaneously, the system at chemical equilibrium fulfils both Eqs. 4 and 5. The standard Gibbs energy of the two reactions, and thus the two equilibrium constants, are calculated from the ideal gas properties of the pure species, N_2O_4, NO_2, NO and O_2, the ideal gas standard molar enthalpy of formation at 298.15 K, the ideal gas standard molar entropy at 298.15 K, and the ideal gas isobaric heat capacity of each species [50], presented in Sect. 2.1.1. The fugacity of each species (real fluid properties) is determined by means of an equation of state presented in Sect. 2.1.2.

2.1.1 Ideal Gas Properties

A large amount of data for the ideal-gas properties of pure N_2O_4, NO_2, NO and O_2 is available in the literature. In this work, it was decided to perform chemical equilibrium calculations considering the standard molar enthalpies of formation at 298.15 K and the standard molar entropies at 298.15 K for the species N_2O_4, NO_2, NO and O_2 reported by NIST-JANAF Thermochemical Tables [52]. These properties are given in Table 1. For completeness, other available values for N_2O_4 and NO_2 are provided in section S1 of the Supplementary Material.

The temperature-dependent correlations for the ideal gas isobaric molar heat capacity of N_2O_4 and NO_2 are taken from Lasala et al. [30], while those for NO and O_2 are from the DIPPR database [53].

2.1.2 Equation of State

Fluid phase properties of the reactive mixture are determined with the cubic Peng-Robinson (PR) equation of state [54]:

$$P(T,v,z) = \frac{RT}{v - b_{\mathrm{m}}} - \frac{a_{\mathrm{m}}}{v\left(v + b_{\mathrm{m}}\right) + b_{\mathrm{m}}\left(v - b_{\mathrm{m}}\right)} \tag{6}$$

where z is the vector of the molar composition, T is the temperature, v is the molar volume, and R is the universal gas constant. The mixture energy a_{m} and co-volume b_{m} parameters are calculated with the athermal version of the advanced EoS/$a_{res}^{E,\gamma}$ mixing rules recalled in Lasala et al. [55–57] and used in the previous paper on N_2O_4 from the same research group [30]:

$$\begin{aligned} b_m &= \sum_{i=1}^{N_{comp}} z_i b_i \\ \frac{a_m}{b_m} &= \sum_{i=1}^{N_{comp}} z_i \frac{a_i}{b_i} \end{aligned} \tag{7}$$

where the pure component energy and co-volume parameters, i.e., a_i and b_i, respectively, are calculated according to the PR equation of state as a function of the critical temperature, pressure and acentric factor of the species forming the system, as shown in Eq. 8.

Table 1 Ideal-gas properties used in this work

	N_2O_4	NO_2	NO	O_2
$\Delta_f H^\circ_{i,298.15\ K}$ / kJ·mol^{-1}	9.080	33.100	90.291	0
$S^\circ_{i,298.15\ K}$ / J·mol^{-1}·K^{-1}	304.376	240.034	210.758	205.147

$$\begin{cases} R = 8.314462618\, J \cdot mol^{-1} \cdot K^{-1} \\ X = \left[1 + \sqrt[3]{4 - 2\sqrt{2}} + \sqrt[3]{4 + 2\sqrt{2}}\right]^{-1} \\ b_i = \Omega_b \dfrac{RT_{c,i}}{P_{c,i}} \text{ with } \Omega_b = \dfrac{X}{X+3} \\ a_i(T) = \Omega_a \dfrac{R^2 T_{c,i}^2}{P_{c,i}} \left[1 + m_i\left(1 - \sqrt{\dfrac{T}{T_{c,i}}}\right)\right]^2 \text{ with } \begin{cases} \Omega_a = \dfrac{8(5X+1)}{49 - 37X} \\ m_i = 0.37464 + 1.54226\omega_i - 0.26992\omega_i^2 \end{cases} \end{cases} \tag{8}$$

For N_2O_4 and NO_2, critical temperatures, pressures and acentric factors were previously calculated from the results of Monte-Carlo simulations in Lasala et al. [30], since those are not experimentally measurable, and are optimized in this work as shown in Sect. 2.4. These properties are given in Table 2, together with the measurable properties of pure NO and O_2 taken from the DIPPR database [53].

2.2 Algorithms Applied for Chemical Equilibrium Calculations

The knowledge of the equilibrium composition of the system is necessary to calculate the thermodynamic properties of the system in its equilibrium state. The composition can be evaluated analytically only for the simplest problems, such as ideal-gas systems [11, 58–62]. The determination of the equilibrium composition in real reactive systems, especially in the case of multiphase equilibria, requires the implementation of specific algorithms.

2.2.1 Single Phase Properties

The single-phase reactions $N_2O_4 \rightleftarrows 2NO_2$ and $2NO_2 \rightleftarrows 2NO + O_2$ or, simultaneously $N_2O_4 \rightleftarrows 2NO_2 \rightleftarrows 2NO + O_2$, take place with the number of degrees of freedom equal to two or three. The generalized Gibbs phase rule and the considered systems [63] gives:

$$v = 2 + c - \varphi - r - s \tag{9}$$

where c, φ and r are, respectively, the number of molecular species, the number of phases, and the number of chemical reactions. The variable s is the number of

Table 2 Initial critical properties and acentric factors used in this work

	T_c, K	P_c, bar	ω	Reference
N_2O_4	484.2	55.9	0.3212	[30]
NO_2	282.2	68.2	0.0565	[30]
NO	180.15	64.8	0.5829	[53]
O_2	154.58	50.43	0.0222	[53]

additional constraints imposed on the system. The resulting variance is presented in Table 3 for the different systems of interest in the present study.

Calculations of chemical equilibrium correspond to the search of intensive equilibrium state variables (temperature, pressure, mole fractions) after specifying a number of independent intensive variables equal to the variance of the system. This problem has been extensively studied in the literature [64, 65]. There are two main strategies: stoichiometric and non-stoichiometric approach. In the stoichiometric approach, the condition of chemical equilibrium, Eq. 1, is considered: the Gibbs energy is minimized with respect to the extent of reaction and without additional constraints (unconstrained problem). The non-stoichiometric approach is based on direct minimization of the Gibbs energy of the system for a specified temperature, pressure and global composition with respect to material balance constraints (constrained problem). In this work, the non-stoichiometric method is applied; specifically, the modified RAND method [66, 67] is implemented to take advantage of quadratic convergence and satisfaction of the material balance constraints at every iteration.

2.2.2 Vapour–Liquid Equilibrium Properties

VLE properties of the general system $N_2O_4 \rightleftarrows 2NO_2 \rightleftarrows 2NO + O_2$ are calculated considering the presence of only the first reaction, $N_2O_4 \rightleftarrows 2NO_2$. It will be shown in Sect. 3.4 that the impact of the second reaction on thermodynamic properties in the VLE domain is negligible.

The reactive system $N_2O_4 \rightleftarrows 2NO_2$ at VLE has only one degree of freedom [30]. This fact means that only one intensive variable (temperature, pressure or the mole fraction of N_2O_4 or NO_2 in either the liquid or gas phase) must be specified in order to perform equilibrium calculations. As a consequence, classical strategies of chemical equilibrium calculations can not be applied. In order to perform simultaneous phase and chemical equilibrium calculations, it is necessary to solve Eq. 10:

$$\begin{cases} \mu_{N_2O_4}^{liq} = \mu_{N_2O_4}^{vap} \\ \mu_{NO_2}^{liq} = \mu_{NO_2}^{vap} \\ \Delta_R G = 0 \end{cases} \tag{10}$$

Table 3 Variance of the systems considered in the present study in the single phase

	$N_2O_4 \rightleftarrows 2NO_2$	$2NO_2 \rightleftarrows 2NO + O_2$	$N_2O_4 \rightleftarrows 2NO_2 \rightleftarrows 2NO + O_2$
c	2	3	4
φ	1	1	1
r	1	1	2
s	0	0(*)	0(*)
υ	**2**	**3(*)**	**3(*)**

(*) If the molar composition of the system presents a stoichiometric relationship between NO and O_2, i.e. $x(O_2) = 2 \cdot x(NO)$, the variable s is equal to 1 and the variance υ is equal to 2

Lasala et al. [30] showed that it is enough to consider a condition of chemical equilibrium for only one of the two coexistent phases: in the case of equilibrium between phases, the condition of chemical equilibrium is automatically reached in the other phase. The implementation of an equation of state to perform calculations allows the replacement of the condition of chemical potential equality ($\mu_i^{\mathrm{liq}} = \mu_i^{\mathrm{vap}}$) by the condition of equal fugacity ($\hat{f}_i^{liq} = \hat{f}_i^{vap}$). However, after this substitution, the molar volumes of the liquid (v^{liq}) and vapour (v^{vap}) appear as two new variables of the system. Therefore, it is necessary to add in the considered system (10) two more equations connecting temperature, pressure, molar volume and composition: the equation of state applicable to both phases. As a result, we obtain a set of five equations, Eq. 11, already presented in Lasala et al. [30] and Molina et al. [68]. Indeed, the same strategy of calculations was successfully performed for the *n*-butane $\rightleftarrows$ isobutane isomerization by Molina et al. [68].

$$\begin{cases} \hat{f}_{N_2O_4}^{\mathrm{liq}}\left(T, v^{\mathrm{liq}}, \boldsymbol{x}\right) = \hat{f}_{N_2O_4}^{\mathrm{vap}}(T, v^{\mathrm{vap}}, \boldsymbol{y}) \\ \hat{f}_{NO_2}^{\mathrm{liq}}\left(T, v^{\mathrm{liq}}, \boldsymbol{x}\right) = \hat{f}_{NO_2}^{\mathrm{vap}}(T, v^{vap}, \boldsymbol{y}) \\ K(T)_R = \frac{1}{P^{\circ}} \prod_{i=N_2O_4,NO_2} \left[\hat{f}_i\left(T, v^{\mathrm{liq}}, \boldsymbol{x}\right)\right]^{\nu_i} \text{ or } K(T)_R = \frac{1}{P^{\circ}} \prod_{i=N_2O_4,NO_2} \left[\hat{f}_i(T, v^{\mathrm{vap}}, \boldsymbol{x})\right]^{\nu_i} \\ P - P_{\mathrm{EoS}}\left(T, v^{\mathrm{liq}}, \boldsymbol{x}\right) = 0 \\ P - P_{\mathrm{EoS}}(T, v^{\mathrm{vap}}, \boldsymbol{y}) = 0 \end{cases} \tag{11}$$

Vectors with molar composition of the liquid and vapour phases are denoted as $\boldsymbol{x} = \left\{x_{\mathrm{NO_2}}, x_{\mathrm{N_2O_4}}\right\} = \left\{x_{\mathrm{NO_2}}, 1 - x_{\mathrm{NO_2}}\right\}$ and $\boldsymbol{y} = \left\{y_{NO_2}, y_{N_2O_4}\right\} = \left\{y_{NO_2}, 1 - y_{NO_2}\right\}$, respectively. If all model parameters are known, system (11) has five equations and six variables: T, P,v^{liq},v^{vap},$x_{\mathrm{NO_2}}$, and $y_{\mathrm{NO_2}}$. Since the number of the degrees of freedom equals one, it is possible to fix one intensive variable and to solve the system for the five unknowns, starting from a reliable initial guess of the solution: in this work, at a specified temperature, system (11) is solved for P,v^{liq},v^{vap},$x_{\mathrm{NO_2}}$, and $y_{\mathrm{NO_2}}$.

In order to calculate the entire VLE curve, calculations are performed in this work from the triple point to the critical point of the system, with a specified temperature-step value. For each temperature, the system of equations is solved numerically with the Newton–Raphson method, and convergence is considered achieved for a maximum value of the residuals lower than 10^{-8}; however, the implementation of this method requires suitable initial guesses. The first point of the curve is solved fixing the triple point temperature (known variable) and solving the system considering as initial guess the solution obtained analytically with the approximation «ideal gas – ideal solution»; to draw the curve at further higher temperatures, the initial guess which is used to solve the system (11) at each temperature step is the result of the previous lower temperature step calculation. Calculations are performed up to the critical point temperature, where molar compositions and molar volumes coincide with each other.

Furthermore, VLE calculations are performed assuming that N_2O_4 and NO_2 do not react, in order to obtain saturated vapour pressures of pure N_2O_4 and pure NO_2,

and the critical line of the binary non-reactive mixture N_2O_4–NO_2. The critical line of the hypothetical non-reactive system N_2O_4–NO_2 is calculated with the method of Cismondi and Michelsen [69], proposed for binary non-reactive systems.

The calculated critical point of the reactive system $N_2O_4 \rightleftarrows 2NO_2$ is then determined as the unique point on the traced non-reactive critical line where the condition of chemical equilibrium (1) is achieved. The unique non-isothermal phase diagram of the reactive $N_2O_4 \rightleftarrows 2NO_2$ system at the coordinates $P - x, y$ is also drawn, and the results of calculations are compared with Monte-Carlo simulations performed in Lasala et al. [30].

2.3 Experimental Data for the System $N_2O_4 \rightleftarrows 2NO_2 \rightleftarrows 2NO + O_2$

This section includes available experimental data for the reactive system $N_2O_4 \rightleftarrows 2NO_2 \rightleftarrows 2NO + O_2$: properties at VLE (critical properties, triple point temperature, saturated pressure, saturated densities of the liquid and vapour states, and enthalpy of vaporization). The properties of the liquid and vapour phases are presented in section S2 of the Supplementary Material.

2.3.1 Critical Properties

Experimental critical data for the considered system [70–82] are presented in Table S3 of the Supplementary Material. Critical temperature data show good agreement: experimental values from different authors differ by no more than one Kelvin, except for the data of Nadejdine [72] and Scheuer [79]. Critical pressures and critical densities are also given in Table S3, and data are in a good agreement with each other. However, the critical temperature and critical density determined by Bennewitz and Windisch [70] should be removed from consideration, the issue of this data source is addressed in Sect. 2.3.4.

2.3.2 Triple Point Temperature

The triple point temperature is necessary as a meaningful starting point for VLE pressure calculations. Experimental data on the triple point temperature are consistent with each other: Whittaker et al. [83] and Giauque and Kemp [84] reported the values 261.85 K and 261.9 K, respectively.

2.3.3 Vapour Pressure at Vapour–Liquid Equilibrium

The vapour–liquid equilibrium pressure of the considered system is very well investigated. Existing sources [13, 71, 74–79, 84–94] and the intervals of measured temperatures and VLE pressures are given in Table S4 of the Supplementary Material. 365 data points are available in the literature, 40 % of which are located in the low-temperature area between the triple point temperature and 300 K. Not all of these data are considered in the model optimization, since some sources show significant deviations from other measurements, i.e., the data of Guye and Drouginine [88] and

Scheuer [79]. Indeed, VLE pressures based on the data of Guye and Drouginine [88] exhibit an inflection point near 273 K. To the knowledge of the authors, it has never been demonstrated that inflection points are excluded for reactive systems; it could be thought that at low temperatures, where the fluid is mostly made of N_2O_4 molecules, the saturation curve of the reactive system $N_2O_4 \rightleftarrows 2NO_2$ overlaps the pure N_2O_4 curve, while as the temperature increases and the reaction proceeds, it approaches the pure NO_2 curve, presenting an inflection in the process. However, none of the subsequent studies have confirmed the anomalous behaviour of the curve based on data of Guye and Drouginine [88]. These data are not in agreement with the other experimental data for VLE pressure [76–78, 84, 87–90], as shown by Kulešov [95]. The calculations carried out in this study are thus conducted without the data from Scheuer [79] and Guye and Drouginine [88]. The final set of VLE pressure data considered in this work included 344 points.

2.3.4 Density at Vapour–Liquid Equilibrium

The sources and main features of the available experimental data on the saturated density of liquid and vapour phases for the reactive system $N_2O_4 \rightleftarrows 2NO_2$ [70, 73, 77–79, 81, 82, 89, 96–99] are presented in Tables S5 and S6 of the Supplementary Material, respectively. Tables S5 and S6 include features of the saturated densities of Reamer and Sage [77], which are not experimental data but estimates obtained from graphical processing of experimental single-phase volumetric data. Data obtained by Bennewitz and Windisch [70] and Scheuer [79], which do not agree very well with other sources, are excluded from other considerations. The final set of density data considered in this work includes 126 points for the saturated liquid phase and 85 points for the saturated vapour phase.

2.3.5 Enthalpy of Vaporization

The enthalpy of vaporization of a pure species is defined as the increase in enthalpy that accompanies the vaporization of a unit of liquid at constant temperature and pressure [100] and the calculation of this property in molar or mass terms is equivalent since the vaporization process does not change the mole number. However, this is not the case for reactive fluids in which, at constant temperature and pressure, the mole number in the liquid phase to be vaporized differs from the one of the vaporised vapour phase (see Supplementary Material, section S4). Considering that the mass of the system does not change, it is advised to present enthalpy of vaporization values on a mass basis.

In contrast to VLE pressures and densities, the enthalpy of vaporization is poorly studied for this reactive system. There are only two articles, containing overall two data: the articles of Giauque and Kemp [84] and Coon [101]. Both references report molar values, specifying the molar mass used for the conversion from mass to molar terms. With this data, it is possible to obtain the relative mass quantities: Giauque and Kemp [84] provide a value of 99 ± 0.1 cal·g^{-1} measured at 294.25 K, while Coon [101] measured a value of 73.3 cal·g^{-1} at 298.1 K.

Other sources containing data on vaporization heat [75, 76, 84, 102, 103] present results of calculations with the Clapeyron equation based on the experimental data for vapour pressure: Devojno and Mišina [102] and Seshadri et al. [103] performed calculations of the mass heat of vaporization with the experimental data for molar volumes of liquid and vapour at saturation; Scheffer and Treub [75, 76] and Giauque and Kemp [84] calculated molar heat of vaporization neglecting the volume of the liquid phase and calculating the molar volume of the vapour phase with equations of state, and evaluated the degree of dissociation from calculations based on the equilibrium constant. Data on molar vaporization heat without any additional data on chemical composition of the system should not be considered.

2.4 Optimization of the Properties of Pure N_2O_4 and NO_2

As described in the Sect. 1, in a previous work from the authors [30], coupling Quantum Mechanics and Monte Carlo simulations allowed to evaluate the thermodynamic properties of individual pure species and to perform a semi-predictive modelling of the reactive system. The term "semi-predictive" means that, although no parameters were optimized in the equation of state applied by Lasala et al. [30], Monte Carlo simulations were based on intermolecular force fields of pure NO_2 and of pure N_2O_4 in turn optimized with experimental data of the reactive system by other authors [104]. Those simulations allowed the estimation of the critical coordinates and acentric factor of the pure components, with a certain degree of uncertainty [30]. To improve the accuracy of phase equilibrium properties resulting from the application of the proposed model [30], this paper proposes to optimise the critical coordinates and acentric factor of NO_2 and of N_2O_4.

2.4.1 Selection of Most Sensitive EoS Input Parameters

As justified by Lasala et al. [30] and shown in Sect. 2.1.2, there are no adjustable binary interaction parameters in our model. The optimization of the model performed in this work consists in the optimal determination of the input properties required to apply the cubic equation of state: critical temperatures, critical pressures and acentric factors of NO_2 and N_2O_4, keeping the ideal gas heat capacities unchanged and equal to the ones proposed by NIST [52]. It is thus possible to identify – a priori – six key parameters: critical temperatures of N_2O_4 and NO_2, critical pressures of N_2O_4 and NO_2, and the acentric factors of N_2O_4 and NO_2.

In order to determine which of these properties should be more specifically optimized, a sensitivity analysis has initially been performed for pure-component critical temperatures, critical pressures, and acentric factors, as well as ideal-gas enthalpies and entropies of reaction at $T = 298.15$ K. To this aim, critical properties and acentric factors calculated in Lasala et al. [30] are initially used, with ideal gas properties provided by NIST [52]. Each parameter is perturbed by ± 10 %, keeping constant the other parameters. For each perturbed set of parameters, the system of

Eq. 11 is solved to trace *T-P* and *T-ρ* diagrams. The most sensible input parameters are then chosen as parameters to be optimised, as described in Sect. 3.1.

2.4.2 Objective Function

The optimization of the parameters mentioned in Sect. 2.4.1 is performed to reproduce at best different available experimental VLE data, considering the following objective function:

$$F = \frac{1}{n_X^{\exp}} \sum_{i=1}^{n_X^{\exp}} e_{X,i}^2 = \frac{1}{n_X^{\exp}} \sum_{i=1}^{n_X^{\exp}} \left(\frac{X_i^{\text{calc}} - X_i^{\exp}}{X_i^{\exp}} \right)^2 \tag{12}$$

where $e_{X,i}$ is the relative deviation of the property X for the i-th experimental point; the summation is performed over experimental data at VLE: phase boundary pressure, densities of saturated liquid and vapour, and coordinates of the critical point (critical temperature and critical pressure), where the indices "calc" and "exp" refer to calculated and experimental values, respectively. The experimental data used for the optimisation are presented in Tables S3–S6 of the Supplementary Material. Quasi-Newton BFGS (Broyden-Fletcher-Goldfarb-Shanno) is used as an optimization method. In order to verify the achievement of a global minimum, each optimization is performed 20 times for different random initializations. The success of the optimization is identified with the low number of points "out of model", determined in accordance with available criteria [105], and low values of MAPE (Mean Absolute Percentage Error, defined as in Eq. 12). The optimisation is performed by modelling the system considering the single reaction $N_2O_4 \rightleftarrows 2NO_2$, while the occurrence of the second one, $2NO_2 \rightleftarrows 2NO + O_2$, is neglected.

2.4.3 Validation of Calculations in the Liquid Phase

Optimized parameters are then used to calculate thermodynamic properties of the system $N_2O_4 \rightleftarrows 2NO_2 \rightleftarrows 2NO + O_2$ in the liquid phase and in the supercritical region at the vicinity of the liquid phase (volumetric and caloric properties), and to validate the model's accuracy. For specified temperatures and pressures (identical to experimental values), the molar composition $\left\{x_{NO_2}, x_{N_2O_4}\right\}$ is calculated by the single-phase RAND method [66, 67] and the molar volume of the liquid phase is returned by the equation of state. Calculated densities are then compared with experimental data, whose references are provided in Table S8 of the Supplementary Material. Calculation of molar concentrations c_i are used to obtain the constants, expressed in terms of molar concentrations at equilibrium in the liquid phase $K_{c,N_2O_4 \rightleftarrows 2NO_2}$, according to Eq. 13, and these results are then compared with experimental data provided in Table S7 of the Supplementary Material.

$$K_{c,N_2O_4 \rightleftarrows 2NO_2} = \frac{c^2_{NO_2}}{c_{N_2O_4}} \tag{13}$$

The enthalpy of the system $N_2O_4 \rightleftarrows 2NO_2$ in the liquid phase is calculated with the formula traditionally implemented for inert systems [106, 107]. The results of calculations, presented in Sect. 3, are compared with experimental data of enthalpy increment presented in Table S9 of the Supplementary Material.

3 Results

This section presents the optimised input parameters and the resulting modelling capability of the equation of state, considering both the single reaction $N_2O_4 \rightleftarrows 2NO_2$ and the complete reactive system $N_2O_4 \rightleftarrows 2NO_2 \rightleftarrows 2NO + O_2$.

3.1 Parametric Analysis and Parameter Optimisation

The calculation of vapour pressure and densities at VLE in the $N_2O_4 \rightleftarrows 2NO_2$ system is firstly performed with critical properties and acentric factors previously calculated [30] from data of MC simulations performed with Brick-CFCMC software

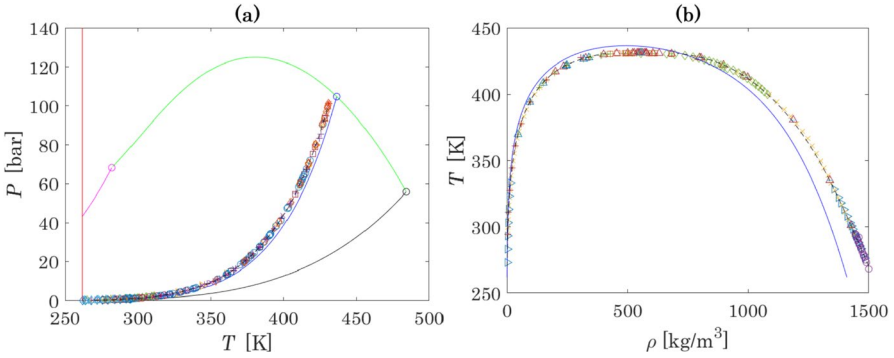

Fig. 1 Results of calculations of VLE properties with the use of critical parameters taken from Lasala et al. [30] and ideal-gas properties from NIST-JANAF database. Figure (a) shows a *P*–*T* plot: pink and black curves are the vaporization curves of pure NO_2 and N_2O_4, respectively; the blue curve is the calculated VLE curve of reactive $N_2O_4 \rightleftarrows 2NO_2$ mixture; the green curve is critical line of the binary (fictitious) inert mixture $N_2O_4 - NO_2$; the red line corresponds to the triple point temperature; the dashed line represents the results obtained with the multiparameter equation of state introduced by Lemmon et al. [110]. Experimental data at the critical point: (✱) Schlinger and Sage [78]. Experimental data on vapour pressure at VLE: (○) Nesterenko (Ed.) [13], (◇) Greben'kov et al. [71], (+) Scheffer and Treub [74–76], (×) Reamer and Sage [77], (▷) Schlinger and Sage [78], (◇) Giauque and Kemp [84], (△) Addison and Sheldon [85], (△) Baume [86], (□) Baume [87], (○) Mittasch et al. [89], (×) Ramsay and Young [90], (+) Selleck et al. [91], (−) Stoddart [92], (▷) Thorpe [93], (□) Cymarnyj [94]. Figure (b) shows a *T*-ρ plot: blue curve – calculated density curve of the reactive $N_2O_4 \rightleftarrows 2NO_2$ mixture; experimental data on densities coexisting at VLE: (△) Polikhronidi et al. [73], (×) Reamer and Sage [77], (+) Schlinger and Sage [78], (□) Curbelev [80], (+) Veržinskaâ et al. [82], (▷) Mittasch et al. [89], (○) Pascal [96], (◇) Greben'kov [97], (−) Amirhanov et al. [98], (△) Veržinskaâ and Curbelev [99] (Color figure online)

Table 4 Optimized parameters of N_2O_4

Parameter	Eq. constant from Lasala et al. [30]	Eq. constant from NIST-JANAF [52]
$T_c(N_2O_4)$	484.1	476.2
$P_c(N_2O_4)$	58.8	59.9

Table 5 MAPE of different properties in the case of non-optimised and optimised input parameters at different equilibrium constants

Property	MAPE (%) of property prediction with eq. constant from NIST-JANAF [52]		MAPE (%) of property prediction with eq. constant from Lasala et al. [30]	
	Non-optimised	**Optimised**	Non-optimised	Optimised
Equilibrium VLE pressure	18.1	**2.4**	11.9	10.7
Density of liquid at VLE	7.2	**3.5**	8.0	3.9
Density of vapor at VLE	26.3	**3.4**	9.3	9.9
Critical temperature	1.2	**0.05**	0.05	0.2
Critical pressure	3.4	**2.7**	7.2	9.3

Bold characters indicate the best optimal model

[108, 109] and ideal gas properties provided by NIST-JANAF [52]. The results are shown in Fig. 1. Input parameters are reported in Table 2. Figure 1 also presents the results obtained with the best available thermodynamic model: the Helmholtz-energy based equation of state introduced by Lemmon et al. [110], based on 111 parameters fitted to accurately represent the thermodynamic properties of the reactive system $N_2O_4 \rightleftarrows 2NO_2 \rightleftarrows 2NO + O_2$.

The influence of each input parameter is then investigated by comparison of the results for the initial and perturbed sets of the parameters, as described in Sect. 2.4.1. Results for each new set of parameters are shown in Figures S1–S4 of the Supplementary Material (section S3). The analysis of Figures S1–S4 shows that $T_c(N_2O_4)$, $P_c(N_2O_4)$, $\Delta_R H^\circ_{298.15\ K}$ and $\Delta_R S^\circ_{298.15\ K}$ have the highest impact on the results of calculations: parameter perturbation can cause the calculated values to change by more than 5 %.

In this work, we have thus decided to optimize only T_c (N_2O_4) and P_c (N_2O_4) and keep other critical properties and acentric factors equal to the values calculated with Brick-CFCMC method in Lasala et al. [30]. $\Delta_R H^\circ_{298.15\ K}$ and $\Delta_R S^\circ_{298.15\ K}$ were not included in the list of optimisation parameters. However, we optimised the critical parameters for N_2O_4 with two sets of $\Delta_R H^\circ_{298.15\ K}$ and $\Delta_R S^\circ_{298.15\ K}$ values: those derived from $\Delta_f H^\circ_{i,298.15\ K}$ and $S^\circ_{i,298.15\ K}$ obtained by Lasala et al. [30] and those derived from $\Delta_f H^\circ_{i,298.15\ K}$ and $S^\circ_{i,298.15\ K}$ published in NIST-JANAF [52].

The optimal T_c (N_2O_4) and P_c (N_2O_4) resulting from the use of those two sets of thermochemical data are reported in Table 4. The MAPE relative to these two optimizations are presented in Table 5 and the resulting thermodynamic diagrams are presented in Fig. 2. For further comparison, Fig. 2 also shows the results obtained with the multiparameter equation of state introduced by Lemmon et al. [110].

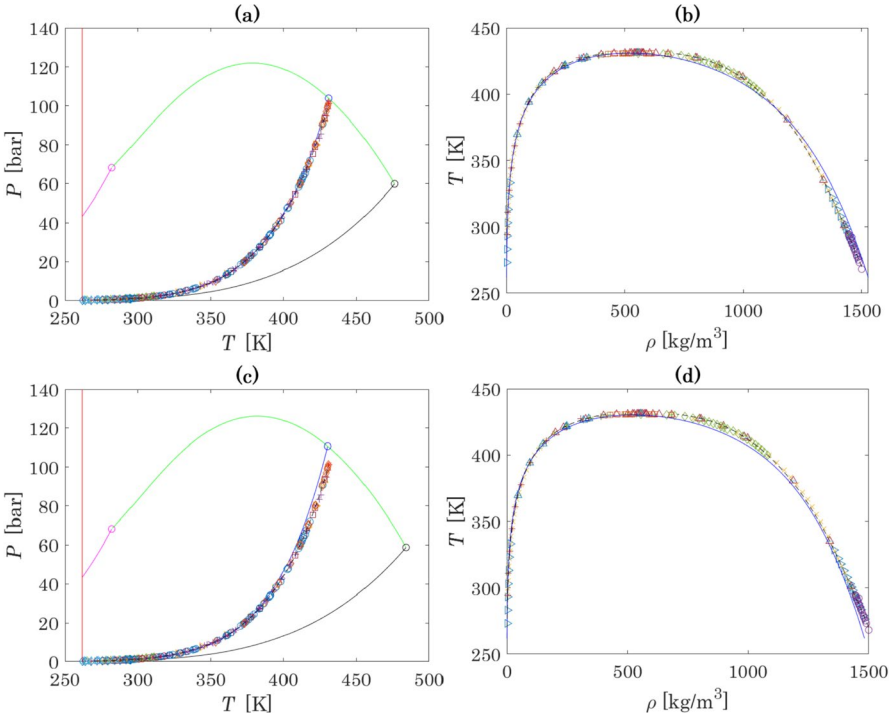

Fig. 2 Results of the optimization of $T_c(N_2O_4)$ and $P_c(N_2O_4)$ for different equilibrium constants: Fig. (a) and (b) correspond to calculations of, respectively, the global phase equilibrium diagram and densities of the coexisting phases with the use of the expression for the equilibrium constant calculated from the NIST-JANAF database [52]. Fig. (c) and (d) correspond to the same calculations performed with the equilibrium constant obtained in Lasala et al. [30]. For more details on symbols and colours, make reference to Fig. 1

The value of the equilibrium constant exerts a significant influence on the results of the calculations. This consideration is not surprising: the error on the equilibrium constant K_R is exponentially related to the error on the value of $\Delta_R G°(T)/RT$, according to Eq. 3. The standard molar enthalpy of formation and standard molar entropy are evaluated by quantum methods and are affected by specific uncertainties that may cause important deviations between the calculated equilibrium constants [111, 112] (for example, DIPPR [53] provides an uncertainty of 3 % for heat of formation and 1 % for absolute entropy of N_2O_4 and NO_2).

The analysis of Fig. 2 and Table 5 leads to the observation that the thermochemical properties that allow the best representation of experimental data (Fig. 2a and b) are the ones proposed in NIST-JANAF [52], and are thus the ones that must be used in the proposed model, together with the associated optimal critical parameters. The final set of parameters proposed in this work is given in Table 6.

One of the main drawbacks of cubic equations of state is their recognised incapability to describe liquid phase densities with low deviations [113]. The results obtained in this work show that the representation of this system is an exception

Table 6 Final set of parameters for N_2O_4 and NO_2

	N_2O_4	NO_2
T_c, K	476.2 (this work)	282.2 ([30])
P_c, bar	59.9 (this work)	68.2 ([30])
ω	0.3212 ([30])	0.0565 ([30])
$\Delta_f H^\circ_{i,298.15\,K}$, kJ·mol^{-1}	33.100 ([52])	9.080 ([52])
$S^\circ_{i,298.15\,K}$, J·mol^{-1}·K^{-1}	240.034 ([52])	304.376 ([52])
$c^\circ_{P,i}(T)$, J·kmol^{-1}·K^{-1} (T, K)	$67574 + 56723 \cdot \left(\frac{723.73/T}{\sinh(723.73/T)}\right)^2 + 13722 \cdot \left(\frac{2093.4/T}{\cosh(2093.4/T)}\right)^2$ ([30])	$33631 + 24566 \cdot \left(\frac{1168.4/T}{\sinh(1168.4/T)}\right)^2 + 10406.5 \cdot \left(\frac{606.3/T}{\cosh(606.3/T)}\right)^2$ ([30])

to the rule, where saturation pressures and densities are represented with unexpected accuracy by a cubic equation of state, without the need of a translation term [114]. Results obtained for vapour pressure, density of saturated liquid and critical density in this work are significantly better than the average performance resulting from the application of an untranslated PR EoS [115].

The resulting non-isothermal phase diagram in the coordinates $P - \{x_1, y_1\}$ is shown in Fig. 3, together with Monte-Carlo simulations obtained by Lasala et al. [30], and the results of the model proposed by Lemmon et al. [110] for comparison. The prediction of the two models is not in very good agreement. However, the lack of experimental compositional data of bubble and dew points does not allow to attest which model performs best. Nevertheless, the attested deviation between the compositions predicted by the two models is expected to have a negligible impact on the size and performance assessment of the engineering processes based on dissociating N_2O_4.

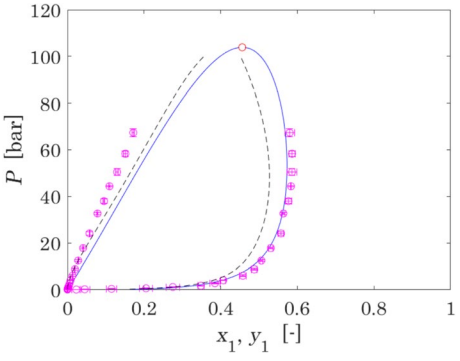

Fig. 3 $P - \{x_1, y_1\}$ diagram of the reactive mixture $N_2O_4 \rightleftarrows 2NO_2$, where NO_2 is component "1": the blue curve represents VLE calculations performed with the model proposed in this work, and the red point is the calculated critical point; pink points with error bars are the results of Monte-Carlo simulations obtained in Lasala et al. [30] by the use of Brick-CFCMC, with their uncertainties; dashed line represents the results obtained with the multiparameter equation of state introduced by Lemmon et al. [110] (Color figure online)

3.2 Validation of the Thermodynamic Model Accuracy

The proposed optimised model has been applied to evaluate different thermodynamic properties of $N_2O_4 \rightleftarrows 2NO_2$ in the liquid phase. The constants calculated in terms of concentration at equilibrium at standard pressure are shown in Fig. 4.

The analysis of Fig. 4 shows that the calculated constants are not in very good agreement with experimental values. However, experimental data on chemical equilibrium are obtained under specific assumptions [61], with reported uncertainties of experimental data that are not always reliable; in addition, impurities and instrument errors could lead to inaccuracies that exceed the uncertainties provided by estimation methods [111]. The equilibrium constants obtained here proposed, in turn, may be biased to compensate for errors in other parameters and model approximations. Therefore, we can state that the optimized model provides a satisfactory description of experimental data on chemical equilibrium of the system investigated.

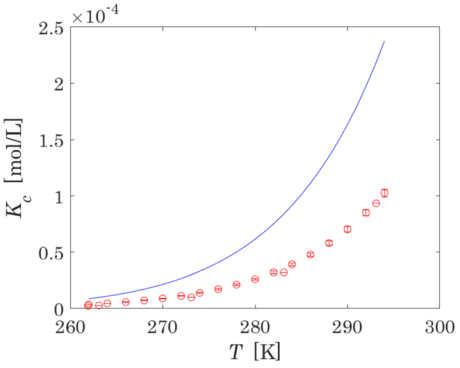

Fig. 4 Constants in terms of concentration at equilibrium of the reaction $N_2O_4 \rightleftarrows 2NO_2$ in the liquid phase. Red points with error bars represent experimental data with their uncertainties [46, 49]; blue line represents calculated values (Color figure online)

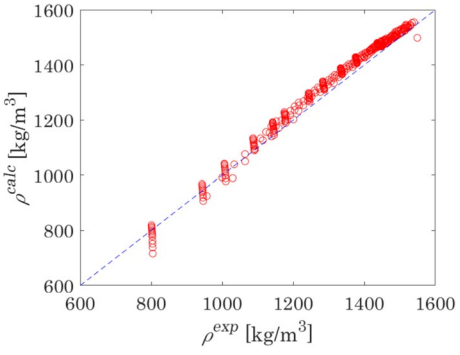

Fig. 5 Plot comparing density calculated with the optimised model versus experimental measurements [77, 93, 94, 117–122] for the single-phase liquid in the reactive $N_2O_4 \rightleftarrows 2NO_2$ system

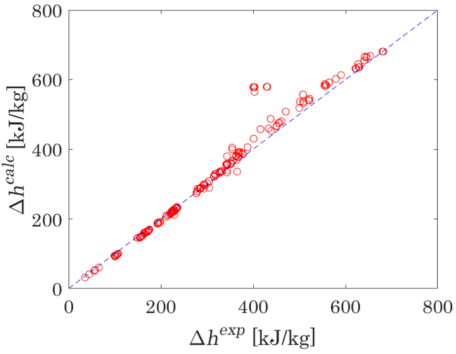

Fig. 6 Plot comparing enthalpy change calculated with the optimised model versus experimental measurements [123–129] for the reactive $N_2O_4 \rightleftarrows 2NO_2$ system

Furthermore, the model is validated on liquid density and liquid enthalpy change, $\Delta h = h(T_{out}, P) - h(T_{in}, P)$, where T_{in} and T_{out} are the inlet and outlet temperatures of the calorimeter and P is the pressure in the calorimeter. The results of calculations versus experimental data are presented in Figs. 5 and 6. The capability of the model to represent these properties is very satisfactory: the MAPE of liquid densities is equal to 2.8 %, which is far below deviations typically observed for non-translated PR EoS (about 7 % [116]); the MAPE of enthalpy changes is equal to 5.2 %, where several points showing the highest deviations lay in the vicinity of the calculated critical point.

The results of the calculations of thermodynamic properties in this work were compared to the results obtained with the Helmholtz energy equation of state by Lemmon et al. [110]. A comparison of the MAPEs obtained with the use of the model presented in this work and by Lemmon et al. is presented in Table 7. These MAPE are calculated considering the same experimental data, whose sources are reported in the Supplementary Material. The comparison demonstrates that, despite its simplicity, the proposed model is an effective and robust method to calculate thermodynamic properties of the considered reactive system in the subcritical region.

Table 7 MAPE of VLE and liquid phase properties of dissociating N_2O_4, calculated with two models

Property	This work	Lemmon et al. [110]
MAPE (%) of properties at VLE		
VLE pressure	2.4	0.6
Saturated liquid density	3.5	1.6
Saturated vapour density	3.4	4.5
MAPE (%) of properties in the liquid phase		
Density	2.9	0.5
Enthalpy	5.2	20.5

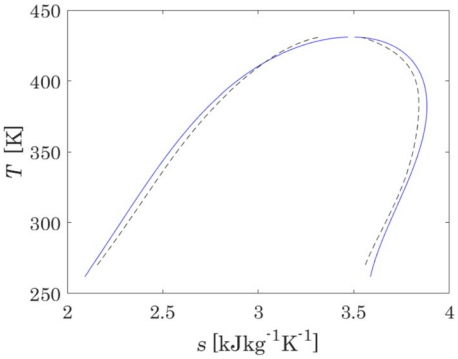

Fig. 7 $T-s$ diagram of the reactive system $N_2O_4 \rightleftarrows 2NO_2$: the blue solid line presents the results obtained with the model optimised in this work; the black dashed line presents the results obtained with the model by Lemmon et al. [110]

Additionally, a $T-s$ diagram, also required for process simulations, is calculated and compared with the model of Lemmon et al. [110]; the results are presented in Fig. 7.

3.3 Properties of Pure N_2O_4

For completeness, since values of input parameters for N_2O_4 (critical temperature and pressure) have changed after optimization, it is worth comparing the impact of these new values on the properties of pure N_2O_4. Calculated values of saturated vapour pressure and density of saturated liquid of N_2O_4 are presented in Fig. 8. Figure 8 shows that at temperatures higher than 350 K, model predictions deviate from Monte Carlo simulation results. However, considering the uncertainty and deviations of Monte Carlo simulations themselves, the modelling result is considered satisfactory.

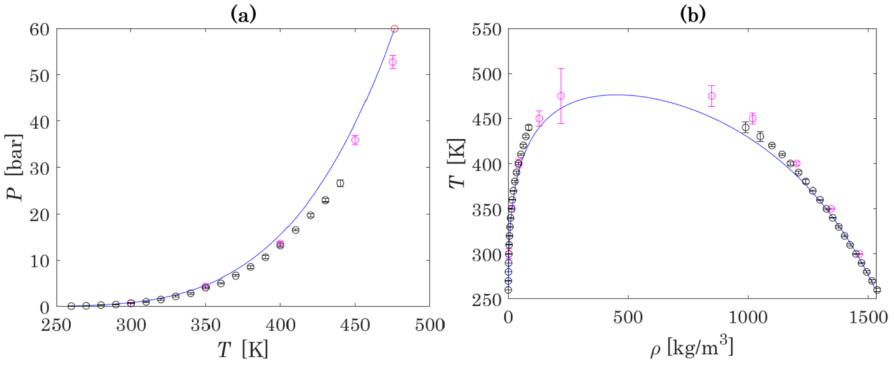

Fig. 8 Saturated vapour pressure (a) and densities at VLE (b) of N_2O_4: the blue curve is based on the results of calculations with the model and parameters obtained in this work, pink points and black points present results obtained in [30] with Gibbs and Brick-CFCMC MC methods, respectively (Color figure online)

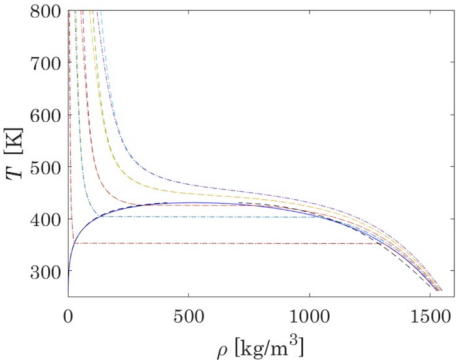

Fig. 9 $T-\rho$ diagram for a selected set of isobars (10, 50, 90, 150 and 200 bar) calculated for the system $N_2O_4 \rightleftarrows 2NO_2$ (dashed lines) and $N_2O_4 \rightleftarrows 2NO_2 \rightleftarrows 2NO + O_2$ (dotted lines). The blue solid line corresponds to results of VLE calculations for optimised parameters (Color figure online)

3.4 Modelling the Full Reactive System $N_2O_4 \rightleftarrows 2NO_2 \rightleftarrows 2NO + O_2$

This section aims to show how the additional consideration of the dissociation of nitrogen dioxide $2NO_2 \rightleftarrows 2NO + O_2$ affects the results of calculations in the vapour phase. The calculations are now performed for the quaternary system $N_2O_4 \rightleftarrows 2NO_2 \rightleftarrows 2NO + O_2$ and compared to the previous case, where only $N_2O_4 \rightleftarrows 2NO_2$ is considered.

This comparison is shown on the $T-\rho$ diagram in Fig. 9. It is specified that, for the quaternary system, equilibrium compositions are computed by the RAND method, as detailed in Sect. 2.2. From a volumetric point of view, it can be concluded that considering, or not, the reaction $2NO_2 \rightleftarrows 2NO + O_2$ does not change the results of calculations in the liquid phase and in the low-temperature vapour region. Therefore, the consideration of only the reaction $N_2O_4 \rightleftarrows 2NO_2$ in the subcritical region, considered in this work during the model optimisation, is proven to be a good assumption. However, at higher temperatures, where the differences between the binary or quaternary representation of the system become more pronounced, the occurrence of the second reaction should also be taken into account.

4 Conclusion

This paper presents an accurate thermodynamic model based on the Peng-Robinson equation of state, coupled with the athermal version of advanced EoS/$a_{res}^{E,\gamma}$ mixing rules, and its optimal parametrisation for the accurate description of the phase equilibrium and volumetric properties of the $N_2O_4 \rightleftarrows 2NO_2$ system.

Reversible dimerization reactions (i.e., $N_2O_4 \rightleftarrows 2NO_2$) exhibit a peculiar behaviour at vapour-liquid equilibrium: the chemical reaction $N_2O_4 \rightleftarrows 2NO_2$ constantly evolves with the modification of temperature, and the experimental determination of the critical properties of pure N_2O_4 and of pure NO_2 is thus not possible. In a previous work [30], those properties were assessed by coupling Monte-Carlo and

Quantum Mechanics to characterise N_2O_4 and NO_2, and it was realised that the use of a different Monte Carlo software leads to non-negligible deviations of resulting critical coordinates.

In continuity with this previous research, the present work aims to optimise those parameters in the variability range observed in Lasala et al. [30] to improve the model's accuracy in the two-phase region. Prior to parameter optimisation, a sensitivity analysis is performed, leading to two main conclusions: (1) the variation of thermochemical ideal gas properties, such as standard molar enthalpy of formation and standard molar entropy, in the uncertainty range characterising the most accurate Quantum Chemistry results, leads to significant deviations of thermodynamic calculations; (2) only the critical properties of N_2O_4 have a non-negligible impact on the calculated VLE properties of reactive mixtures. In this work, the ideal gas thermochemical properties are thus set to the values proposed by NIST [52, 130], the critical coordinates of NO_2 are fixed equal to the values obtained in Lasala et al. [30], while the critical coordinates of the N_2O_4 are optimised.

The model's optimisation is performed by considering the occurrence of the only reaction $N_2O_4 \rightleftarrows 2NO_2$. Furthermore, the validity of such an assumption is confirmed by modelling the full reactive system $N_2O_4 \rightleftarrows 2NO_2 \rightleftarrows 2NO + O_2$ at VLE and attesting the negligible variation of the calculations due to the inclusion of the higher-temperature reaction $2NO_2 \rightleftarrows 2NO + O_2$. Moreover, the optimised model is finally validated based on liquid densities and enthalpy variations, and compared with the results obtained with the Helmholtz energy equation of state recently proposed by Lemmon et al. [110].

Despite its simplicity, the here-parametrised cubic equation of state enables the description of VLE densities and pressures, with an excellent degree of accuracy, which is quantified in this paper. The obtained equation of state thus enables the reliable design and optimisation of chemical, power generation and refrigeration processes based on $N_2O_4 \rightleftarrows 2NO_2$.

Supplementary Information The online version contains supplementary material available at https://doi.org/10.1007/s10765-025-03565-x.

Acknowledgments This work received funding from the European Research Council (ERC) under the European Union's Horizon Europe research and innovation program (grant agreement No. 101040994). The authors thank Prof. Jean-Noël Jaubert for sharing his knowledge in chemical engineering thermodynamics and Prof. Romain Privat for sharing the software used in this work to calculate the critical line as well as for his contribution to the development of the code used for chemical equilibrium calculations.

Author Contributions KS acquired and analysed the available experimental data, and performed the main investigation. KS and SL developped the software to perform the calculations with the model presented in this work. DVM supervised the experimental data review process. EL provided the documents and codes which have enabled to apply a reference accurate multiparameter equation of state and thus to benchmark the model here presented. VD provided part of the experimental data used in the optimisation process. SL supervised the work and acquired the financial support for the project leading to this publication. All authors contributed to the editing of the text.

Funding This work was supported by European Research Council (grant agreement No. 101040994).

Data Availability Data will be made available upon request.

Declarations

Conflict of interest The authors declare no competing interests.

References

1. M.J. Lighthill, Dynamics of a dissociating gas. Part I. Equilibrium flow. J. Fluid Mech. **2**, 1–32 (1957). https://doi.org/10.1017/S0022112057000713
2. V.P. Bubnov, A.M. Matûnin, V.B. Nesterenko, Thermodynamic analysis of cycles using chemically reacting gases as the working system. Vescì Akad. Navuk BSSR Seryâ Fiz.-Teh. Navuk 15–18 (1966)
3. A.K. Krasin, Ed. Dissociiruûšie Gazy kak Teplonositeli i Rabočie Tela Èenergetičeskih Ustanovok: Materialy Vsesoûznoj Konferencii [Dissociating Gases as Heat-Transfer Media and Working Substances in Power Plants: Proceedings of All-Union Conference], Nauka i Tehnika, Minsk, 1970.
4. K. Kesavan, The use of dissociating gases as the working fluid in thermodynamic power conversion cycles, PhD Thesis, Nuclear Science and Engineering Division, Carnegie-Mellon University, 1978. https://www.proquest.com/openview/c0920507f648498a5b1c8afcabf69ede (access restricted).
5. G. Angelino, Performance of N_2O_4 gas cycles for solar power applications. Proc. Inst. Mech. Eng. **193**, 313–320 (1979). https://doi.org/10.1243/PIME_PROC_1979_193_033_02
6. K. Kesavan, J.F. Osterle, Split-flow nuclear gas turbine cycle using dissociating N_2O_4, ASME, 1982. https://appliedmechanics.asmedigitalcollection.asme.org/GT/proceedings/GT1982/79580/V003T08A008/232993 (accessed February 1, 2025).
7. H.M. Huang, R. Govind, Use of dissociating gases in Brayton cycle space power systems. Ind. Eng. Chem. Res. **27**, 803–810 (1988). https://doi.org/10.1021/ie00077a015
8. B. Nufer, A summary of NASA and USAF hypergolic propellant related spills and fires, in: SpaceOps 2010 Conf., American Institute of Aeronautics and Astronautics, Huntsville, Alabama, 2010. https://doi.org/10.2514/6.2010-1994.
9. S.M. Davis, N. Yilmaz, Advances in hypergolic propellants: ignition, hydrazine, and hydrogen peroxide research. Adv. Aerosp. Eng. **2014**, 1–9 (2014). https://doi.org/10.1155/2014/729313
10. G.P. Sutton, O. Biblarz, *Rocket Propulsion Elements*, 7th edn. (Wiley, Hoboken, 2001)
11. A.K. Krasin, V.B. Nesterenko, Eds. Termodinamičeskie i Transportnye Svojstva Himičeski Reagiruûših Gazovyh Sistem. Čast' I [Thermodynamic and Transport Properties of Chemically Reacting Gaseous Systems. Part I], Nauka i Tehnika, Minsk, 1967.
12. A.K. Krasin, Ed. Thermodynamic and transport properties of chemically reacting gaseous systems. Part II (Trans. by Foreign Technology Division Wright-Patterson Air Force Base, Ohio), Nauka i Tehnika, Minsk, 1971. https://apps.dtic.mil/sti/tr/pdf/AD0756597.pdf. Accessed 1 Nov 2024
13. V.B. Nesterenko, Ed. Teplofizičeskie Svojstva Četyrekhokisi Azota [Thermophysical Properties of Nitrogen Tetroxide], Nauka i Tehnika, Minsk, 1982.
14. M.A. Bazhin, V.P. Bubnov, V.B. Nesterenko, N.M. Shiryaeva, Optimisation of parameters of power plants using dissociating working fluids. Translated by J. Miller, Foreign Technology Division, Air Force Systems Command U. S. Air Force, Ohio, 1972. https://apps.dtic.mil/sti/tr/pdf/AD0743688.pdf. Accessed 1 Nov 2024

15. L.I. Kolyhan, V.B. Nesterenko, Teploobmen v Dissociiruûsem Teplonositele Četyrehokisi Azota [Heat Exchange in Dissociating Heat-Transfer Media Dinitrogen Tetroxide], Nauka i Tehnika, Minsk, 1977.
16. V.B. Nesterenko, A.A. Mihalevič, B.E. Tverkovkin, Bystrye Reaktory i Teploobmennye Apparaty AÈS s Dissociiruûsim Teplonositelem (Metody Teplofizičeskogo Rasčeta) [Fast Reactors and Heat Exchangers of NPP with Dissociating Heat-Transfer Media (Methods of Thermophysical Calculations)], Nauka i Tehnika, Minsk, 1978.
17. S. Lasala, R. Privat, O. Herbinet, P. Arpentinier, D. Bonalumi, J.-N. Jaubert, Thermo-chemical engines: unexploited high-potential energy converters. Energy Convers. Manag. **229**, 113685 (2021). https://doi.org/10.1016/j.enconman.2020.113685
18. A. Barakat, Comprendre l'Impact des Fluides de Travail Chimiquement Réactifs dans les Cycles Thermodynamiques, PhD Thesis, Université de Lorraine, 2024. https://theses.fr/s300808. Accessed 1 Nov 2024
19. J.P. Irving, J.M. Smith, Heat transfer in a chemically reacting system (nitrogen tetroxide-dioxide). AIChE J. **7**, 91–96 (1961). https://doi.org/10.1002/aic.690070122
20. R.R. Furgason, J.M. Smith, Enthalpy and heat capacity of N_2O_4-NO_2 at pressure above one atmosphere. J. Chem. Eng. Data **7**, 528–529 (1962). https://doi.org/10.1021/je60015a025
21. S.S.T. Fan, D.M. Mason, Properties of the system $N_2O_4 \leftrightarrows 2NO_2 \leftrightarrows 2NO + O_2$. J. Chem. Eng. Data **7**, 183–186 (1962). https://doi.org/10.1021/je60013a007
22. V.B. Nesterenko, L.V. Mišina, Calculation of the isobaric heat capacity of dissociating nitrogen tetroxide at equilibrium in a wide range of temperatures at moderate pressures. Vescì Akad. Navuk BSSR Seryâ Fiz.-Teh. Navuk 33–38 (1965)
23. V.B. Nesterenko, B.E. Tverkovkin, Calculation of the isobaric heat capacity of chemically reacting system taking into account kinetics of chemical reactions. Vescì Akad. Navuk BSSR Seryâ Fiz.-Teh. Navuk 20–30 (1966)
24. R.A. Svehla, R.S. Brokaw, Thermodynamic and transport properties for the $N_2O_4 \leftrightarrows 2NO_2 \leftrightarrows 2NO + O_2$ system. Lewis Research Center, Cleveland, Ohio, 1966. https://ntrs.nasa.gov/api/citations/19660008882/downloads/19660008882.pdf.
25. K.P. Coffin, C. O'Neal, Experimental thermal conductivities of the $N_2O_4 \rightleftarrows 2NO_2$ system. National Advisory Committee for Aeronautics, Cleveland, Ohio, 1958. https://ntrs.nasa.gov/api/citations/19930085092/downloads/19930085092.pdf.
26. R.S. Brokaw, Correlation of turbulent heat transfer in a tube for the dissociating system $N_2O_4 \rightleftarrows 2NO_2$. National Advisory Committee for Aeronautics, Washington, 1958. https://ntrs.nasa.gov/citations/19930090182.
27. A.A. Bilyk, Û.G. Kotelevskij, L.V. Mišina, L.V. Sviridova, B.D. Timofeev, Experimental investigation of the thermal conductivity of dissociating nitrogen tetroxide in a wide range of temperatures and pressures. Vescì Akad. Navuk BSSR Seryâ Fiz.-Energ. Navuk 114–123 (1971)
28. V.B. Nesterenko, B.E. Tverkovkin, A.B. Veržinskaâ, Heat exchange in chemically reacting equilibrium system $N_2O_4 \rightleftarrows 2NO_2$. Vescì Akad. Navuk BSSR Seryâ Fiz.-Teh. Navuk 42–49 (1967)
29. K. Zhang, Y. Shen, C. Duwig, Identification of heat transfer intensification mechanism by reversible N_2O_4 decomposition using direct numerical simulation. Int. J. Heat Mass Transf. **182**, 121946 (2022). https://doi.org/10.1016/j.ijheatmasstransfer.2021.121946
30. S. Lasala, K. Samukov, H. Mert Polat, V. Lachet, O. Herbinet, R. Privat, J.-N. Jaubert, O. Moultos, K. de Ras, T.J.H. Vlugt, Application of thermodynamics at different scales to describe the behaviour of fast reacting binary mixtures in vapour-liquid equilibrium. Chem. Eng. J. **483**, 148961 (2024). https://doi.org/10.1016/j.cej.2024.148961
31. M. Binotti, C. Invernizzi, P.G. Iora, G. Manzolini, Innovative fluids for gas power cycles coupled with solar tower systems. AIP Conf. Proc. **2033**, 070001 (2018). https://doi.org/10.1063/1.5067087
32. N.N. Greenwood, A. Earnshaw, Nitrogen dioxide, NO_2, and dinitrogen tetroxide, N_2O_4, in *Chemistry of the Elements*, 2nd edn. (Butterworth-Heinemann, Boston, 1997), pp.455–458
33. K. Jones, Nitrogen dioxide and dinitrogen tetroxide, in *The Chemistry of Nitrogen*. (Elsevier, Amsterdam, 1973), pp.340–356. https://doi.org/10.1016/B978-0-08-018796-9.50017-8
34. S.H. Bauer, Historiography of a very fast gas reaction: a case history that spanned about 12 decades. Chem. Rev. **102**, 3893–3904 (2002). https://doi.org/10.1021/cr0204045
35. M.R. Gustavson, Kinetics of fast reactions rates of the NO_2-N_2O_4 reaction from heat capacity lag data, PhD Thesis, The Department of Chemistry, Cornell University, 1953. https://apps.dtic.mil/sti/tr/pdf/AD0008892.pdf. Accessed 1 Nov 2024

36. L.V. Mišina, V.B. Nesterenko, V.V. Petrunenko, V.K. Fedosova, About chemical relaxation times in the systems $N_2O_4 \rightleftarrows 2NO_2$ and $2NO_2 \rightleftarrows 2NO + O_2$. Vescì Akad. Navuk BSSR Seryâ Fiz.-Energ. Navuk 85–90 (1969)
37. V.S. Belânin, N.I. Gorbunova, E.E. Špil'rajn, About calculations of chemical relaxation time in gas systems, in: Dissociiruûšie Gazy Kak Tepl. Rab. Tela Ènerg. Ustanov. Mater. III Vses. Konf. Čast II Dissociating Gases Heat-Transf. Media Work. Subst. Power Plants Proc. III -Union Conf. Part II, Heat and Mass Transfer Institute of the National Academy of Sciences of Belarus, Minsk, 1973: pp. 159–169.
38. V.S. Belânin, Chemical relaxation times of decomposition reactions nitrogen tetroxide and nitrogen dioxide in the gas phase. Vescì Akad. Navuk BSSR Seryâ Fiz.-Energ. Navuk 95–100 (1977)
39. M. Fiedler, P. Hess, High precision study of chemical relaxation in the system N_2O_4=$2NO_2$ by photoacoustic resonance spectroscopy. J. Chem. Phys. **93**, 8693–8702 (1990). https://doi.org/10.1063/1.459256
40. H.-J. von Bauer, M. Arlt, H. Hoffmann, Schallabsorption in flüssigem N_2O_4 infolge Relaxation des Dissoziationsgleichgewichts. Acta Acust. **17**, 98–101 (1966)
41. T. Katō, Molecular dynamics simulation of liquid N2O4⇌2NO2 by orientation-sensitive pairwise potential. III. Reaction dynamics. J. Chem. Phys. **120**, 829–838 (2004). https://doi.org/10.1063/1.1630291
42. J.T. Cundall, XCII—dissociation of liquid nitrogen peroxide. J. Chem. Soc. Trans. **59**, 1076–1089 (1891). https://doi.org/10.1039/CT8915901076
43. T. Soné, On the magnetic susceptibility of six nitrogen oxides. Sci. Rep. Tohoku Imp. Univ. First Ser. Math. Phys. Chem. **11**, 139–157 (1922)
44. A.G. Whittaker, Magnetic susceptibility study of the liquid phase equilibrium $N_2O_4 \rightleftharpoons 2NO_2$ in pure nitrogen tetroxide. J. Chem. Phys. **24**, 780–783 (1956). https://doi.org/10.1063/1.1742609
45. C.M. Steese, A.G. Whittaker, Spectrophotometric study of the liquid-phase equilibrium $N_2O_4 \rightleftharpoons 2NO_2$ in pure nitrogen tetroxide. J. Chem. Phys. **24**, 776–779 (1956). https://doi.org/10.1063/1.1742608
46. P. Gray, P. Rathbone, Dissociation of liquid dinitrogen tetroxide; Henry's law coefficients, heats and entropies of solution, and the thermodynamics of homolytic dissociation in the pure liquid. J. Chem. Soc. (1958). https://doi.org/10.1039/jr9580003550
47. D.W. James, R.C. Marshall, Electron spin resonance study of the dinitrogen tetroxide-nitrogen dioxide system. J. Phys. Chem. **72**, 2963–2966 (1968). https://doi.org/10.1021/j100854a048
48. T.F. Redmond, B.B. Wayland, Dimerization of nitrogen dioxide in solution: a comparison of solution thermodynamics with the gas phase. J. Phys. Chem. **72**, 1626–1629 (1968). https://doi.org/10.1021/j100851a040
49. A.J. Vosper, The dissociation of dinitrogen tetroxide in the liquid phase. J. Chem. Soc. Inorg. Phys. Theor. (1970). https://doi.org/10.1039/j19700002191
50. P. Atkins, J. De Paula, *Physical Chemistry*, 9th edn. (W.H. Freeman and Company, New York, 2010)
51. J.P. O'Connell, J.M. Haile, *Thermodynamics: Fundamentals for Applications* (Cambridge University Press, New York, 2005)
52. NIST-JANAF Thermochemical Tables, (2013). https://janaf.nist.gov/. Accessed 1 Nov 2024
53. DIPPR® Project 801 Database, (2023). https://www.aiche.org/dippr.
54. D.-Y. Peng, D.B. Robinson, The characterization of the heptanes and heavier fractions for the GPA Peng-Robinson programs, Gas Processors Association, 1978.
55. S. Lasala, P. Chiesa, R. Privat, J.-N. Jaubert, VLE properties of CO_2–based binary systems containing N_2, O_2 and Ar: experimental measurements and modelling results with advanced cubic equations of state. Fluid Phase Equilib. **428**, 18–31 (2016). https://doi.org/10.1016/j.fluid.2016.05.015
56. S. Lasala, P. Chiesa, R. Privat, J.-N. Jaubert, Measurement and prediction of multi-property data of CO_2-N_2-O_2-CH_4 mixtures with the "Peng-Robinson + Residual Helmholtz energy-based" model. Fluid Phase Equilib. **437**, 166–180 (2017). https://doi.org/10.1016/j.fluid.2017.01.016
57. S. Lasala, Advanced cubic equations of state for accurate modelling of fluid mixtures. application to CO_2 capture systems. PhD Thesis, Politecnico di Milano, 2016. https://www.politesi.polimi.it/handle/10589/117757
58. D.N. Underwood, D.E. Webster, The effect of pressure on the dissociation of dinitrogen tetroxide. Sch. Sci. Rev. **60**, 309–311 (1978)

59. I.A. Leenson, Approaching equilibrium in the N_2O_4-NO_2 system: a common mistake in textbooks. J. Chem. Educ. **77**, 1652 (2000). https://doi.org/10.1021/ed077p1652
60. W.E. Price, D.W. Griffith, S.R. Wilson, Thermodynamics of the NO_2-N_2O_4 equilibrium by FTIR: an APCELL experiment. Aust. J. Educ. Chem. **67**, 14–17 (2007)
61. M.G. Dunn, K. Wark, J.T. Agnew, Determination of the equilibrium constant for the gas-phase dissociation of nitrogen tetroxide by infrared absorption techniques. J. Chem. Phys. **37**, 2445–2449 (1962). https://doi.org/10.1063/1.1733025
62. E.-G. Kang, S.-J. Kang, An analysis and improvement of the experiment about the effect of pressure on the equilibrium of the NO_2-N_2O_4 system. J. Korean Chem. Soc. **47**, 283–291 (2003). https://doi.org/10.5012/jkcs.2003.47.3.283
63. J.M. Smith, H.C. Van Ness, M.M. Abbott, M.T. Swihart, *Introduction to Chemical Engineering Thermodynamics*, 8th edn. (McGraw-Hill Education, New York, 2018)
64. W.R. Smith, R.W. Missen, *Chemical Reaction Equilibrium Analysis: Theory and Algorithms* (Wiley, New York, 1982)
65. F. van Zeggeren, S.H. Storey, *The Computation of Chemical Equilibria* (Cambridge University Press, Cambridge, 1970)
66. C. Tsanas, Simultaneous chemical and phase equilibrium calculations with non-stoichiometric methods. PhD Thesis, Technical University of Denmark, 2018. https://backend.orbit.dtu.dk/ws/files/181125809/ChristosTsanas_online.pdf. Accessed 1 Nov 2024
67. C. Tsanas, E.H. Stenby, W. Yan, Calculation of multiphase chemical equilibrium by the modified RAND method. Ind. Eng. Chem. Res. **56**, 11983–11995 (2017). https://doi.org/10.1021/acs.iecr.7b02714
68. M.J. Molina, S.B. Rodriguez-Reartes, M.S. Zabaloy, A theoretical study on the simultaneous vapor-liquid and chemical equilibria in a highly restricted system. Fluid Phase Equilib. **557**, 113439 (2022). https://doi.org/10.1016/j.fluid.2022.113439
69. M. Cismondi, M.L. Michelsen, Global phase equilibrium calculations: critical lines, critical end points and liquid–liquid–vapour equilibrium in binary mixtures. J. Supercrit. Fluids **39**, 287–295 (2007). https://doi.org/10.1016/j.supflu.2006.03.011
70. K. Bennewitz, J.J. Windisch, Eine neue Methode zur Bestimmung der Dichte von aggressiven Flüssigkeiten unter hohem Druck, im besonderen der kritischen Dichte von Stickstofftetroxyd. Z. Für Phys. Chem. **166A**, 401–415 (1933). https://doi.org/10.1515/zpch-1933-16640
71. A.Ž. Greben'kov, V.P. Curbelev, S.V. Limarenko, Phase equilibrium parameters of nitrogen tetroxide and their asymptotic behavior in the critical point region. I. Vapour Pressure, Vescì Akad. Navuk BSSR Seryâ Fiz.-Energ. Navuk (1985) 56–60.
72. A. Nadejdine, La Détermination de la Température Critique dans les Tubes Opaques. Bull. Acad. Imp. Sci. St-Petersbourg **30**, 327–330 (1886)
73. N.G. Polikhronidi, R.G. Batyrova, I.M. Abdulagatov, Isochoric heat capacity measurements of nitrogen tetroxide system at temperatures between 410 and 484 K and pressures up to 35 MPa. Fluid Phase Equilib. **175**, 153–174 (2000). https://doi.org/10.1016/S0378-3812(00)00457-X
74. F.E.C. Scheffer, J.P. Treub, Determinations of vapour tensions of nitrogen tetroxide. Proc. KNAW 14 (1911) 536–549. https://dwc.knaw.nl/toegangen/digital-library-knaw/?pagetype=publDetail&pId=PU00013111
75. F.E.C. Scheffer, J.P. Treub, Determinations of the vapour tension of nitrogen tetroxide. Proc. KNAW 15 (1912) 166–178. https://dwc.knaw.nl/toegangen/digital-library-knaw/?pagetype=publDetail&pId=PU00012961
76. F.E.C. Scheffer, J.P. Treub, Die Dampfdruckkurve des Stickstofftetroxyds. Z. Für Phys. Chem. **81U**, 308–332 (1913). https://doi.org/10.1515/zpch-1913-8116
77. H.H. Reamer, B.H. Sage, Volumetric behavior of nitrogen dioxide in the liquid phase. Ind. Eng. Chem. **44**, 185–187 (1952). https://doi.org/10.1021/ie50505a052
78. W.G. Schlinger, B.H. Sage, Volumetric behavior of nitrogen dioxide. Ind. Eng. Chem. **42**, 2158–2163 (1950). https://doi.org/10.1021/ie50490a042
79. O. Scheuer, Preliminary report of the examination of the physical and chemical properties of pure gases and binary mixtures. Anz. Österr. Akad. Wiss. **48**, 304–307 (1911)
80. V.P. Curbelev, Determination of the critical temperature of dissociating nitrogen tetroxide. Vescì Akad. Navuk BSSR Seryâ Fiz.-Energ. Navuk 58–60 (1984)
81. V.P. Curbelev, Temperature dependency of density on the liquid-gas coexistence curve for NO_2-NO Solutions in the extended critical region (experimental determination and tables of thermodynamic

properties). Abstract of a PhD thesis in Technical Sciences, Institute of Nuclear Energy of the Belarus Academy of Sciences, 1986.
82. A.B. Veržinskaâ, V.P. Curbelev, P.M. Klepatskij, Impact of nitrogen monoxide on the shape of the coexistence curve of N_2O_4 in the vicinity of the critical point liquid-vapor. in: 5th -Union Sch. Appl. Math. Methods Descr. Stud. Phys.-Chem. Equilibria Ext. Abstr. Rep. Part II, Novosibirsk, 1985: pp. 120–123.
83. A.G. Whittaker, R.W. Sprague, S. Skolnik, G.B.L. Smith, Vapor pressures and freezing points of the system nitrogen tetroxide—nitric oxide. J. Am. Chem. Soc. **74**, 4794–4797 (1952). https://doi.org/10.1021/ja01139a021
84. W.F. Giauque, J.D. Kemp, The entropies of nitrogen tetroxide and nitrogen dioxide. The heat capacity from 15°K to the boiling point. The heat of vaporization and vapor pressure. The equilibria N_2O_4=$2NO_2$=2NO+O_2. J. Chem. Phys. **6**, 40–52 (1938). https://doi.org/10.1063/1.1750122
85. C.C. Addison, J.C. Sheldon, 373 Vapour pressures of mixtures of dinitrogen tetroxide with donor and with non-donor organic solvents comparison with some nitrosyl chloride systems. J. Chem. Soc. (1957). https://doi.org/10.1039/JR9570001937
86. G. Baume, M. Robert, Some properties of pure dinitrogen trioxide and of its solution in nitrogen peroxide. Comptes Rendus Hebd. Séances Académie Sci. **169**, 968–970 (1919). https://doi.org/10.1259/jrs.1912.0009
87. G. Baume, M. Robert, A glass manometer with elastic walls. Comptes Rendus Hebd. Séances Académie Sci. **168**, 1199–1201 (1919). https://doi.org/10.1259/jrs.1912.0009
88. P.-A. Guye, G. Drouginine, Nouvelle Révision du Poids Atomique de l'Azote. Analyse Exacte du Peroxyde d'Azote. J. Chim. Phys. **8**, 473–514 (1910). https://doi.org/10.1051/jcp/1910080473
89. A. Mittasch, E. Kuss, H. Schlueter, Dichten und Dampfdrucke von wäßrigen Ammoniaklösungen und von flüssigem Stickstofftetroxyd für das Temperatur-gebiet 0° bis 60°. Z. Für Anorg. Allg. Chem. **159**, 1–36 (1927). https://doi.org/10.1002/zaac.19261590102
90. W. Ramsay, S. Young, On evaporation and dissociation. Part I. Philos. Trans. R. Soc. Lond. **177**, 71–122 (1886). https://doi.org/10.1098/rstl.1886.0003
91. F.T. Selleck, H.H. Reamer, B.H. Sage, Volumetric and phase behavior of mixtures of nitric oxide and nitrogen dioxide. Ind. Eng. Chem. **45**, 814–819 (1953). https://doi.org/10.1021/ie50520a046
92. E.M. Stoddart, The effect of drying on the vapour pressure of dinitrogen tetroxide and the vapour density of dinitrogen trioxide. J. Chem. Soc. (1945). https://doi.org/10.1039/jr9450000448
93. T.E. Thorpe, On the relation between the molecular weights of substances and their specific gravities when in the liquid state. J. Chem. Soc. Trans. **37**, 141–225 (1880). https://doi.org/10.1039/CT8803700141
94. V.A. Cymarnyj, Density of liquid nitrogen tetroxide at temperatures 300–500 K and pressures up to 600 Bar, N. 2165-70. Deposited in VINITI, Odessa, 1970.
95. G.G. Kulešov, Thermodynamic properties of dissociating nitrogen tetroxide. I. Vapor Pressure Curve. Vescì Akad. Navuk BSSR Seryâ Fiz.-Teh. Navuk 53–59 (1967)
96. P. Pascal, M. Garnier, Relations between nitrogen peroxide and nitric acid. Bull. Société Chim. Fr. **25**, 309–321 (1919)
97. A.Ž Greben'kov, V.P. Curbelev, A.B. Veržinskaâ, V.B. Nesterenko, Study of the thermodynamic properties of nitrogen dioxide in the wide range of the critical point. Teplofiz. Svojstva Veŝestv Mater. **27**, 41–53 (1989)
98. H.I. Amirhanov, N.G. Polihronidi, B.G. Alibekov, R.G. Batyrova, Isochoric heat capacity of nitrogen tetroxide and the effect of dissociation on the form of $C_v(T)$. Vescì Akad. Navuk BSSR Seryâ Fiz.-Energ. Navuk 113–118 (1981)
99. A.B. Veržinskaâ, V.P. Curbelev, Experimental study of T_s-ρ_s parameters of dissociated heat-transport medium on the basis of N_2O_4 by the method of Quasi-Static Thermogram's in the range of temperature 373 K to T_c. Vescì Akad. Navuk BSSR Seryâ Fiz.-Energ. Navuk 43–46 (1982)
100. B.N. Roy, *Fundamentals of Classical and Statistical Thermodynamics* (Wiley, Hoboken, 2002)
101. E.D. Coon, The heat of vaporization and of dissociation of nitrogen tetroxide. Proc. N. D. Acad. Sci. 7 (1953) 46–48. https://www.ndacadsci.org/historical-information. Accessed 15 April 2024
102. A.N. Devojno, L.V. Mišina, On the calculation of vaporization heat of liquid nitrogen tetroxide. Vescì Akad. Navuk BSSR Seryâ Fiz.-Teh. Navuk 31–34 (1966)
103. D.N. Seshadri, D.S. Viswanath, N.R. Kuloor, Thermodynamic properties of the system N_2O_4⇆$2NO_2$⇆2NO+O_2. AIChE J. **16**, 420–425 (1970). https://doi.org/10.1002/aic.690160319

104. E. Bourasseau, V. Lachet, N. Desbiens, J.-B. Maillet, J.-M. Teuler, P. Ungerer, Thermodynamic behavior of the CO_2 + NO_2/N_2O_4 mixture: a Monte Carlo simulation study. J. Phys. Chem. B **112**, 15783–15792 (2008). https://doi.org/10.1021/jp8068255
105. J.-N. Jaubert, Y. Le Guennec, A. Piña-Martinez, N. Ramirez-Velez, S. Lasala, B. Schmid, I.K. Nikolaidis, I.G. Economou, R. Privat, Benchmark database containing binary-system-high-quality-certified data for cross-comparing thermodynamic models and assessing their accuracy. Ind. Eng. Chem. Res. **59**, 14981–15027 (2020). https://doi.org/10.1021/acs.iecr.0c01734
106. J. Gmehling, M. Kleiber, B. Kolbe, J. Rarey, *Chemical Thermodynamics for Process Simulation*, Second, Completely Revised and Enlarged. (Wiley, Weinheim, 2019)
107. J.-W. Qian, R. Privat, J.-N. Jaubert, P. Duchet-Suchaux, Enthalpy and heat capacity changes on mixing: fundamental aspects and prediction by means of the PPR78 cubic equation of state. Energy Fuels **27**, 7150–7178 (2013). https://doi.org/10.1021/ef401605c
108. R. Hens, A. Rahbari, S. Caro-Ortiz, N. Dawass, M. Erdős, A. Poursaeidesfahani, H.S. Salehi, A.T. Celebi, M. Ramdin, O.A. Moultos, D. Dubbeldam, T.J.H. Vlugt, Brick-CFCMC: open source software for Monte Carlo Simulations of phase and reaction equilibria using the continuous fractional component method. J. Chem. Inf. Model. **60**, 2678–2682 (2020). https://doi.org/10.1021/acs.jcim.0c00334
109. H.M. Polat, H.S. Salehi, R. Hens, D.O. Wasik, A. Rahbari, F. De Meyer, C. Houriez, C. Coquelet, S. Calero, D. Dubbeldam, O.A. Moultos, T.J.H. Vlugt, New features of the open source Monte Carlo software brick-CFCMC: thermodynamic integration and hybrid trial moves. J. Chem. Inf. Model. **61**, 3752–3757 (2021). https://doi.org/10.1021/acs.jcim.1c00652
110. E.W. Lemmon, A.H. Harvey, J.M. Young, Thermodynamic Model for the Reactive Mixture Comprising Dinitrogen Tetroxide (N_2O_4), Nitrogen Dioxide (NO_2), Nitric Oxide (NO), and Oxygen (O_2), Report to NASA from Applied Chemicals and Materials Division, National Institute of Standards and Technology, Boulder, 2022. Available at request from refprop@nist.gov.
111. B.E. Poling, J.M. Prausnitz, J.P. O'Connell, *The Properties of Gases and Liquids*, 5th edn. (McGraw-Hill, New York, 2001)
112. I.A. Uspenskaâ, Applied aspects of modern chemistry. 6. Physical Chemistry. Chemical Thermodynamics, (2021). https://teach-in.ru/lecture/2021-09-25-Uspenskaya. Accessed 1 Nov 2024
113. J.-N. Jaubert, R. Privat, *Thermodynamic Models for Chemical Processes: Design, Develop, Analyse and Optimize* (ISTE Press Ltd - Elsevier Inc, London, 2021)
114. R. Privat, J.-N. Jaubert, Y. Le Guennec, Incorporation of a volume translation in an equation of state for fluid mixtures: which combining rule? Which effect on properties of mixing? Fluid Phase Equilib. **427**, 414–420 (2016). https://doi.org/10.1016/j.fluid.2016.07.035
115. A. Pina-Martinez, R. Privat, J.-N. Jaubert, D.-Y. Peng, Updated versions of the Generalized Soave α-function suitable for the Redlich-Kwong and Peng-Robinson equations of state. Fluid Phase Equilib. **485**, 264–269 (2019). https://doi.org/10.1016/j.fluid.2018.12.007
116. A. Piña-Martinez, R. Privat, J.-N. Jaubert, Use of 300,000 pseudo-experimental data over 1800 pure fluids to assess the performance of four cubic equations of state: SRK, PR, -RK, and -PR. AIChE J. **68**, e17518 (2022). https://doi.org/10.1002/aic.17518
117. C.C. Addison, B.C. Smith, Volume changes on mixing organic liquids with dinitrogen tetroxide: comparison with sulphur dioxide systems. J. Chem. Soc. (1958). https://doi.org/10.1039/jr9580003664
118. W. Ramsay, J. Shields, LXXXI—the molecular complexity of liquids. J. Chem. Soc. Trans. **63**, 1089–1109 (1893). https://doi.org/10.1039/CT8936301089
119. W.R. Bousfield, III—mixtures of nitrogen peroxide and nitric acid. J. Chem. Soc. Trans. **115**, 45–55 (1919). https://doi.org/10.1039/CT9191500045
120. L.S. Vitûk, Èksperimental'naya Metodika i Rezul'taty Issledovaniya Termodinamičeskikh Svojstv Agressivnykh i Vysokoviskoznykh Veshchestv Kak Rabochikh Tel Ènergeticheskikh Ustanovok [Experimental Methodology and Results of the Determination of Thermodynamic Properties of Aggressive and Viscous Compounds as Working Fluids of Power Plants, Abstract of a PhD thesis in Technical Sciences, Odessa Technological Institute of Refrigeration Industry, 1982.
121. L.S. Vitûk, E.A. Golovskij, Experimental investigation of density and isobaric heat capacity of nitrogen tetroxide and solutions based on it. Teplofiz. Svojstva Vešestv Mater. 40–48 (1988)
122. L.S. Vitûk, E.A. Golovskij, A.G. Tabačnikov, Experimental study of thermodynamic properties of nitrogen tetroxide at 230–330 K. Deposited in ONIITEKHim, SPSTL 39 Khp-D80, (1980).

123. Û.A. Sarumov, Issledovanie Èntal′pii Azotnogo Tetraksida v Širokoj Oblasti Parametrov Sostoâniâ [Investigation of Enthalpy of Nitrogen Tetroxide in a Wide Range of State Parameters], Abstract of a PhD thesis in Technical Sciences, Moscow Energy Institute of the Order of Lenin, 1969.
124. A.E. Šejndlin, N.I. Gorbunova, Û.A. Sarumov, Experimental investigation of enthalpy of chemically reacting system $N_2O_4 \leftrightarrows 2NO_2 \leftrightarrows 2NO + O_2$. Dokl. Akad. Nauk SSSR 186 (1969) 817–819. https://www.mathnet.ru/links/b618abf372d953d4811aeb9a595d0417/dan34675.pdf
125. A.E. Šejndlin, N.I. Gorbunova, Û.A. Sarumov, Corrections to the article "experimental investigation of enthalpy of chemically reacting system $N_2O_4 \leftrightarrows 2NO_2 \leftrightarrows 2NO + O_2$" (Doklady Akademii Nauk SSSR, 186(4), 1969). Dokl. Akad. Nauk SSSR 188 (1969) 8. https://www.mathnet.ru/links/ee8d87bbf438cbdfad446aa19d314cd0/dan34919.pdf
126. A.E. Šejndlin, N.I. Gorbunova, Û.A. Sarumov, Enthalpy of nitrogen tetroxide in the near-critical region of the parameters of state. Teplofiz. Vysok. Temp. 11 (1973) 1192–1197. https://www.mathnet.ru/links/ad86d58a9bd82c9671a4d585c4eb8611/tvt9976.pdf
127. A.E. Šejndlin, N.I. Gorbunova, V.M. Simonov, Experimental enthalpy data of nitrogen tetroxide. Teplofiz. Vysok. Temp. 12 (1974) 666–669. https://www.mathnet.ru/links/392bc0b823e30348eaf9121a2d4d64b6/tvt9397.pdf
128. A.E. Šejndlin, N.I. Gorbunova, V.M. Simonov, Enthalpy of dissociating nitrogen tetroxide at pressures up to 30 MPa and temperatures up to 782 K. Teplofiz. Vysok. Temp. 15 (1977) 767–771. https://www.mathnet.ru/links/125b26aa45934caf22230266a7698229/tvt7139.pdf.
129. V.M. Simonov, Èksperimental′noe Issledovanie Kaloričeskih Svojstv Četyrehokisi Azota i Difenil′noj Smesi [Experimental Investigation of Caloric Properties of Nitrogen Tetroxide and Diphenyl Mixture], Abstract of a PhD thesis in Technical Sciences, Institute of High Temperatures, Academy of Sciences of the USSR, 1977.
130. M.W. Chase Jr., Monograph No. 9. NIST-JANAF thermochemical tables. Fourth Edition., J. Phys. Chem. Ref. Data (1998) 1–1951. https://srd.nist.gov/JPCRD/jpcrdM9.pdf. Accessed 1 Nov 2024

Authors and Affiliations

Konstantin Samukov[1] · David Vega-Maza[2] · Eric W. Lemmon[3] · Vladimir Diky[3] · Silvia Lasala[1]

✉ Silvia Lasala
silvia.lasala@univ-lorraine.fr

[1] Université de Lorraine, CNRS, LRGP, 54000 Nancy, France

[2] Group of Energy, Economy and Systems Dynamics (GEEDS), Bioeconomy Research Institute BioEcoUVa, University of Valladolid, Paseo del Cauce 59, 47011 Valladolid, Spain

[3] Applied Chemicals and Materials Division, National Institute of Standards and Technology, Boulder, CO 80305-3337, USA